

Degrade is Upgrade: Learning Degradation for Low-light Image Enhancement

Kui Jiang^{1,†}, Zhongyuan Wang¹, Zheng Wang¹, Peng Yi¹, Xiao Wang¹, Yansheng Qiu¹, Chen Chen², Chia-Wen Lin³

¹Wuhan University, ²University of North Carolina at Charlotte, ³National Tsing Hua University

[†]kuijiang_1994@163.com

Abstract

Low-light image enhancement aims to improve an image's visibility while keeping its visual naturalness. Different from existing methods, which tend to accomplish the enhancement task directly, we investigate the intrinsic degradation and relight the low-light image while refining the details and color in two steps. Inspired by the color image formulation (diffuse illumination color plus environment illumination color), we first estimate the degradation from low-light inputs to simulate the distortion of environment illumination color, and then refine the content to recover the loss of diffuse illumination color. To this end, we propose a novel Degradation-to-Refinement Generation Network (DRGN). Its distinctive features can be summarized as 1) A novel two-step generation network for degradation learning and content refinement. It is not only superior to one-step methods, but also is capable of synthesizing sufficient paired samples to benefit the model training; 2) A multi-resolution fusion network to represent the target information (degradation or contents) in a multi-scale cooperative manner, which is more effective to address the complex unmixing problems. Extensive experiments on both the enhancement task and the joint detection task have verified the effectiveness and efficiency of our proposed method, surpassing the SOTA by 0.95dB in PSNR on LOL1000 dataset and 3.18% in mAP on ExDark dataset. **Our code is available at <https://github.com/kuijiang0802/DRGN>**

1. Introduction

Low-light conditions cause a series of visibility degradation and even sometimes destroy the color or content of the image. Such signal distortion and detail loss often lead to the failure of many computer vision tasks, such as detection [32] and identification [48]. Restoring low-light degraded images and converting them to normally exposed high-quality ones is considered as low-light enhancement.

Early low-light enhancement works mainly focus on contrast enhancement to recover the visibility of dark regions [15, 20, 17]. Since the hand-crafted priors and as-

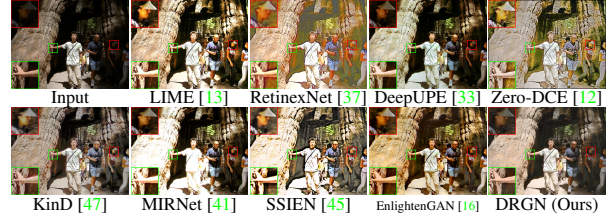


Figure 1. Results of different low-light image enhancement methods. RetinexNet [37], KinD [47], DeepUPE [33] and EnlightenGAN [16] light up the image contents, but cause severe color distortion. LIME [13], Zero-DCE [12], MIRNet [41] and SSiEN [45] tend to produce over-exposed images. Our DRGN generates more realistic and credible textures with visually pleasing contrast.

sumptions are introduced for specific scenes or degradation conditions, these techniques [18] are less effective on scenarios when the predefined models do not hold. Recently, deep learning frameworks have emerged as a promising solution to low-light image enhancement [5, 49, 6]. The existing methods can be roughly divided into two categories in terms of the imaging models under low-light conditions.

Scheme One: An observed low-light image I_L is featured as a superposition of a normal-light image I with some perturbations I_N (noise, exposure, etc.) through a special combination manner $\theta(\cdot)$, defined as

$$I_L = \theta(I, I_N). \quad (1)$$

Given I_L , the goal of low-light image enhancement is to predict I . When $\theta(\cdot)$ is simplified as the pixel-wise summation [11], the effort is to learn the perturbation I_N and then subtract it from the observed image I_L . Some methods [26, 8, 30] also attempt to directly estimate the optimal approximation of I . However, these methods rely heavily on the abundant data, innovative architectures and training methods, but ignore the intrinsic degradation itself, thereby resulting in unsatisfactory and unnatural contents in texture, color, contrast, etc.

Scheme Two: The low-light image I_L is mathematically modeled as a combination of the reflectance I_R and illumination I_T component through Eq. 2:

$$I_L = I_R \circ I_T, \quad (2)$$

where \circ denotes the element-wise product. With this kind of scheme, an image can be enhanced either by estimating and adjusting the illumination map [23, 33], or by learning joint features of these two components [47]. It is known as the Retinex based method [20, 31, 37]. These methods follow the layer decomposition paradigm and show impressive results in stretching contrast and removing noise in some cases, but still have three problems. 1) Traditional models rely on properly enforced priors and regularization. 2) Deep RetinexNets require a large number of paired training samples. 3) The enhanced reflectance I_R is often treated as the normal-light image [40], which often fails to produce high-fidelity and naturalness results due to the gap between the ideal situation and reality with simplified imaging models.

In summary, there are two main drawbacks of these two schemes. First, their performances *heavily rely on the diversity and quality of synthetic training samples*. Second, they *simplify the imaging model* when coping with the enhancement task, thus *sacrificing representation precision*, especially when being trained on a small dataset. More specifically, since the degradation additionally damages the texture, color, and contrast of normal-light images, we argue that subtracting the perturbation I_N from its low-light input I_L directly (**scheme one**) cannot fully recover multiple kinds of fine details and the color distribution (refer to MIRNet [41] in Figure 1). Meanwhile, adjusting the illumination map to enhance reflectance I_R (**scheme two**) cannot fully keep the visual naturalness of the predicted normal-light image (refer to RetinexNet [37] and DeepUPE [33] in Figure 1).

In light of the color image formulation, an image is composed of the diffuse illumination color and the environment illumination color, determined by the light source, albedo (material), environment light, noise, *etc.* [38]. We thus promote **scheme one** by considering the blending relations between the normal-light image I and the degradation I_D , denoted as $f(I_D, I)$. The newly designed low-light image generation process can be typically modeled as

$$I_L = I_D + I + f(I, I_D) = I_D + \psi(I, I_D). \quad (3)$$

We argue $(I, f(I_D, I))$ represents the intrinsic manifold projection from I to I_L via degradation I_D . We formulate this complex mapping as a high-dimensional non-analytic transfer map $\psi(I, I_D)$ since there is no explicit analytic function to present the blending relations caused by the albedo (material) (I), environment light, noise, *etc.* (I_D).

By doing so, we believe the degradation I_D can be learned from the low-light input I_L via a degradation generator (DeG), formulated as $\phi(I_L)$. Thus, given I_L , we use Eq. 4 to predict the normal-light image I as

$$I = \psi^{-1}(I_L - \phi(I_L)). \quad (4)$$

To alleviate the learning difficulty, our enhancement task is

then decomposed into two stages: (1) simulating the degradation I_D via DeG, and (2) refining the color and contrast information by a refinement generator (ReG) which is parameterized by $\psi^{-1}(\cdot)$ (learning the inverse representation of $\psi(\cdot)$). More specifically, inspired by the impressive results of GAN in image synthesis and translation [10, 3, 14], we train a parametric generator to learn the degradation factors from the low-light input in the first stage, denoted as $\phi(I_L)$. Note that simulated degradation factors are also applied to another referenced high-quality dataset to generate synthetic low-light samples to mitigate the limitation of sample monotonicity and repetitiveness (More details on the data generation are described in Sec. 2.3). Meanwhile, we produce the base enhancement result I_B by removing the predicted degradation from the low-light input. Thus, the second stage takes I_B as input, and applies ReG to estimate the inverse transformation matrix to further refine the color and textural details.

DeG is implemented with a multi-resolution fusion strategy because the degradation always acts on various texture richness levels. We thus propose a multi-resolution fusion network (MFN) to learn the joint representation of multi-scale features. In the second stage, ReG shares the same architecture as DeG for simplicity, since the cooperative representation among the multi-scale features also contributes more to the recovery of image textures.

Our main contributions are summarized as follows:

- We propose to decompose and characterize the low-light degradation. Thanks to the degradation generator, it can augment an arbitrary number of paired samples using a small synthetic dataset, and achieves impressive performance and robustness. Our proposed degradation formulation can be easily extended to other enhancement tasks, to help get rid of paired dataset collection.
- We propose a multi-resolution fusion network (MFN) to characterize the target information (degradation or content) in a coordinated manner. Based on this, we construct a novel two-stage Degradation-to-Refinement Generation Network (DRGN) by cascading DeG and ReG for low-light image enhancement task.
- Besides achieving impressive enhancement performance (surpassing KinD [47] by 2.13dB in PSNR on Test148 dataset [16]), our method also outperforms the current representative methods on the joint low-light image enhancement and detection tasks on the ExDark [25] and NightSurveillance [34] datasets.
- We also introduce two novel low/normal-light datasets (COCO24700 for training and COCO1000 for evaluation) based on COCO [4] dataset, which can be used for the joint low-light image enhancement and detection tasks under extreme night-time degradation scenarios (we provide the details of these two datasets in the *Supplementary Material*).

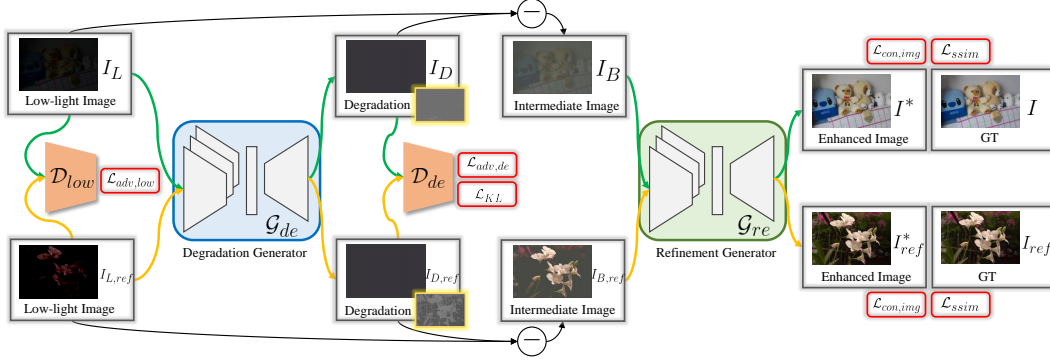


Figure 2. Architecture of Degradation-to-Refinement Generation Network (DRGN). It consists of two subnetworks to tackle degradation estimation and content refinement, respectively. A degradation generator (DeG) learns degradation I_D from the low-light input I_L in the first stage, and produces the base enhanced result I_B by removing I_D . Then, a refinement generator (ReG) takes I_B as input and produces the refined prediction (I^*) of the normal-light image (I). We also apply DeG to generate the synthetic paired samples $[I_{L,ref}, I_{ref}]$ to augment the sample space to help train these two generators.

2. Method

Figure 2 shows the overall pipeline of our proposed low-light enhancement model – Degradation-to-Refinement Generation Network (DRGN). The objective of DRGN is mainly two-fold: one is to train a degradation generator (DeG) $\mathcal{G}_{de} \mapsto \phi(\cdot)$ to simulate the degradation from low-light inputs. The other is to estimate the inverse transformation matrix with a refinement generator (ReG) $\mathcal{G}_{re} \mapsto \psi^{-1}(\cdot)$ to refine color and textures with the augmented dataset by applying the predicted degradation priors.

2.1. Degradation Generator

Let I_L , I , and I_{ref} respectively denote the low-light input, normal-light image, and high-quality reference image (not in the paired training dataset). In the first stage, we learn the degradation through a generative model where all involved parameters can be inferred in a data-driven manner. Specifically, given a low-light input I_L , we train a degradation generator (DeG) to predict the degradation I_D from I_L , i.e., $I_D = \mathcal{G}_{de}(I_L)$. Thus we can generate the synthetic low-light image $I_{L,ref}$ by combining I_D and I_{ref} . Moreover, we produce the degradation prediction $I_{D,ref}$ from $I_{L,ref}$ using the same generator DeG. More details about the data augmentation are described in Sec. 2.3.

Recall that the degradation style of the input I_L and the synthetic low-light image $I_{L,ref}$ should be shared, we regularize both the predicted degradation prior $[I_D, I_{D,ref}]$ and the low-light image pair $[I_L, I_{L,ref}]$ to be close. We introduce the generative adversarial loss [21] and degradation consistency loss (the KL Divergence) to train both DeG and the discriminator. Here, the generative adversarial loss between the low-light input and synthetic low-light image is defined as

$$\mathcal{L}_{adv,low} = -\log \mathcal{D}_{low}(I_L) - \log(1 - \mathcal{D}_{low}(I_{L,ref})). \quad (5)$$

In addition, the constraints on the predicted degradation pri-

ors $[I_D, I_{D,ref}]$ are expressed as

$$\begin{aligned} \mathcal{L}_{adv,de} &= -\log \mathcal{D}_{de}(I_D) - \log(1 - \mathcal{D}_{de}(I_{D,ref})), \\ \mathcal{L}_{kl} &= \sum p(I_D) \log \frac{p(I_D)}{p(I_{D,ref})}, \end{aligned} \quad (6)$$

where $p(\cdot)$ denotes the target distribution. By setting α to 10^{-5} [21] to balance the GAN losses and consistency loss, the total loss in the first stage is given by

$$\mathcal{L}_{DeG} = \alpha \times (\mathcal{L}_{adv,low} + \mathcal{L}_{adv,de}) + \mathcal{L}_{kl}. \quad (7)$$

2.2. Refinement Generator

We design the refinement generator (ReG) in the second stage using the same architecture of DeG for convenience. In the first stage, we also produce the base enhanced result I_B by removing I_D from the low-light input I_L . Thus ReG takes I_B as input and learns to refine the contrast and textural details. More importantly, except for the original sample pairs $[I_B, I]$, we also generate additional paired images $[I_{B,ref}, I_{ref}]$ for sample augmentation in the first stage. With the enrichment and augmentation of training samples, a more robust image enhancement model can be achieved. The procedures in the second stage can be formulated as

$$I^* = \mathcal{G}_{re}(I_B), I_{ref}^* = \mathcal{G}_{re}(I_{B,ref}), \quad (8)$$

where I^* and I_{ref}^* are the predicted normal-light images via ReG. Unlike the adversarial loss in the first stage, we introduce the content loss (the Charbonnier penalty function [19]) and the SSIM [36] loss between the predicted normal-light image and the high-quality ground truth to guide the optimization of ReG. The loss functions are expressed as

$$\begin{aligned} \mathcal{L}_{con,img} &= \sqrt{(I^* - I)^2 + \epsilon^2} + \sqrt{(I_{ref}^* - I_{ref})^2 + \epsilon^2}, \\ \mathcal{L}_{ssim} &= SSIM(I^*, I) + SSIM(I_{ref}^*, I_{ref}), \\ \mathcal{L}_{ReG} &= \mathcal{L}_{con,img} + \lambda \times \mathcal{L}_{ssim}, \end{aligned} \quad (9)$$

where λ is used to balance the loss terms, and experimentally set as -0.2 . The penalty coefficient ε is set to 10^{-3} .

2.3. Data Augmentation

Previous semi- or un-supervised methods [16, 12, 39] can remove the dependence on the synthetic training samples and learn to restore illumination, color, and contrast adaptively. However, these methods cannot guarantee the signal fidelity and good visual quality simultaneously without the correct guidance of paired supervision. Given a synthetic paired dataset $\mathcal{S} = \{I, I_L\}$ and a high-quality reference dataset $\mathcal{R} = \{I_{ref}\}$, we train a generator to learn the degradation I_D from each I_L in the first stage.

Meanwhile, we adopt the superimposition to fuse I_D and the referred image I_{ref} (arbitrary samples in the high-quality dataset \mathcal{R} but not in the training dataset) to synthesize the low-light image $I_{L,ref}$. According to Eq. 3, it should be $I_{L,ref} = I_D + \psi(I_{ref}^*, I_D)$, where I_{ref}^* denotes the **strictly high-quality** version of I_{ref} , and $\psi(I_{ref}^*)$ is equal to I_{ref} , generated via $\psi(\cdot)$ and I_D . However, due to the lack of I_{ref}^* , we adjust the degradation mapping of $I_{L,ref}$ since low-light image $I_{L,ref}$ and its high-quality version are not one-to-one correspondence to each other. As shown in Figure 2, $I_{L,ref}$ is reformulated as $I_{L,ref} = I_{D,ref} + \psi(I_{ref}, I_{D,ref})$, which strictly fits the definition in Eq. 3. To maintain the diversity and reality of the degradation, we introduce GAN loss and consistency loss to regularize both predicted degradation $[I_D, I_{D,ref}]$ and low-light image pair $[I_L, I_{L,ref}]$ to have similar distributions.

Overall, the aforementioned procedure leads to a new paired dataset $\mathcal{T} = \{I_{ref}, I_{L,ref}\}$ during training. Therefore, our sample space consists of the original sample dataset \mathcal{R} and the new synthetic dataset \mathcal{T} . Our degradation learning and data augmentation scheme is more like a transfer learning of degradation patterns from the normal-light sample domain to the low-light image domain. To better understand the degradation learning in our proposed study, we show the examples of the predicted degradation and the synthetic low-light images in the *Supplementary Material*.

2.4. Multi-resolution Fusion Network

Decomposing a complex task into several sub-problems and further learning their cooperative representation to yield a final solution is an effective scheme to promote the model performance [29, 9]. To this end, we propose to decompose the learning task (including degradation learning and content refinement) into multiple sub-spaces, and construct a multi-resolution fusion network (MFN) to represent the target information in a multi-scale collaborative manner, as demonstrated in Figure 3.

Taking the procedure of degradation learning in DeG for instance, we first generate the image pyramid from the low-light input via Gaussian sampling kernel $G(\cdot)$, and adopt

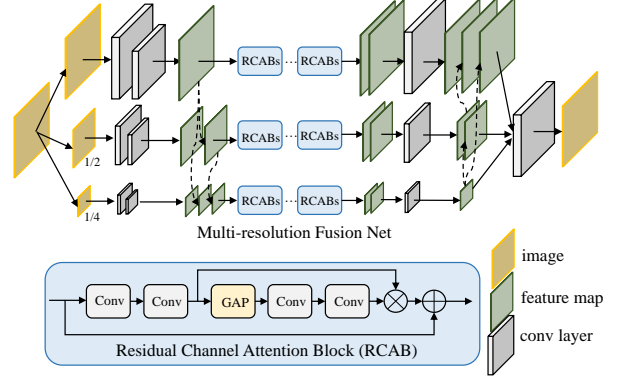


Figure 3. Pipeline of multi-resolution fusion network.

initial convolutions [46] to project the input into the feature space to extract initial features f_{ini}^i , expressed as

$$f_{ini}^i = \mathcal{H}_{ini}^i(G(I_L)), i \subseteq [1, n], \quad (10)$$

where n and i denote the sampling number and the corresponding i_{th} pyramid layer. In particular, the Gaussian sampling is activated except $i = 1$. Before passing f_{ini}^i into the backbone network, we sample the features of high-level branches with strided convolutions, and aggregate them with the features of lower-level branches to form the multi-scale representation (MSR), formulated as

$$f_{msr}^i = \mathcal{H}_{msr}^i(f_{ini}^i, f_{ini}^j), j \subseteq [1, i], \quad (11)$$

where $\mathcal{H}_{msr}^i(\cdot)$ denotes i_{th} -layer multi-scale fusion. After that, we apply the residual group $\mathcal{H}_{RG}^i(\cdot)$ composed of several cascaded residual channel attention blocks (RCABs), each containing multiple RCABs to build deep feature representations [46], as shown in Figure 3. A 1×1 convolution is followed to perform the long-term fusion among the output and input of the residual group. The procedures above can be expressed as

$$f_{long}^i = \mathcal{H}_1^i([\mathcal{H}_{RG}^i(f_{msr}^i), f_{msr}^i]). \quad (12)$$

Through the n -layer pyramid network, we obtain n outputs. To better characterize the degradation, we utilize the deconvolution layer to up-sample the outputs of low-level pyramid layer, and then perform the multi-scale fusion with high-level features via a 1×1 convolution. Consequently, a reconstruction layer $\mathcal{H}_{rec}(\cdot)$ with the filter size of 3×3 is used to project the output of MFN back to the image space. The overall procedure can be summarized as

$$I_D = \mathcal{H}_{rec}(\mathcal{H}_{msr}^j(f_{long}^j, f_{long}^1)), j \subseteq [2, n]. \quad (13)$$

3. Experiments

We carry out extensive experiments on synthetic and real-world low-light image datasets to evaluate the performance of our proposed DRGN. Eight representative

low-light enhancement algorithms are compared, including prior-based LIME [13], learning-based MIRNet [41], KinD [47], DeepUPE [33], RetinexNet [37], reference-free method Zero-DCE [12], SSIEN [45] and EnlightenGAN [16]. Three popular full-reference image quality metrics, including Peak Signal to Noise Ratio (PSNR), Structural Similarity (SSIM) and Feature Similarity (FSIM) [43], are employed for performance evaluation on synthetic datasets. We also conduct additional experiments on real-world low-light datasets and adopt three no-reference quality metrics (*i.e.*, Naturalness Image Quality Evaluator (NIQE) [28], Spatial-Spectral Entropy-based Quality (SSEQ) index [24] and user study scores) for evaluation. Moreover, we conduct object and pedestrian detection under extreme low-light scenarios to demonstrate the impact of low-light image enhancement on high-level vision tasks.

3.1. Implementation Details

Data Collection. Following the setting in RetinexNet [37], we use the LOL dataset for training, which contains 500 low/normal-light image pairs (480 for training and 20 for evaluation). The competing methods are also trained on LOL using their publicly released codes for a fair comparison. Similar to [37, 47], we evaluate our model and the other methods on three widely used synthetic low-light datasets: *LOL1000* [37], *Test148* [16] and *VOC144* [8]. Besides, we also collect 63 real-world low-light samples from [22, 27], namely *Real63*, for evaluation. Finally, a synthetic low-light dataset (COCO1000), a real-world low-light dataset (ExDark [25]) and a video surveillance dataset (NightSurveillance [34]) are used to verify the performance on both image low-light enhancement and detection tasks.

Experimental Setup. In our baseline, the pyramid layer is empirically set to 3, corresponding to the number of RCABs and RCAB depths of [2, 3, 4] and [3, 3, 3], respectively, in the residual group. The training images are cropped to non-overlapping 96×96 patches to obtain the sample pairs. The training samples are augmented via standard augmentation strategies, *i.e.*, scaling and horizontal flipping. We use the Adam optimizer with a batch size of 16 for training DRGN on a single NVIDIA Titan Xp GPU. The learning rate is initialized to 5×10^{-4} and then attenuated by 0.9 every 6,000 steps. After 60 epochs less than 180 thousand iterations on training datasets, we obtain the optimal solution with the above settings. Specifically, we train DeG for the first 20 epochs and then optimize ReG for the rest 40 epochs.

3.2. Ablation Study

Basic Components. Since the proposed DRGN involves multiple enhancement strategies, including the degradation learning (DL), data augmentation (DA), and multi-scale representation (MSR), we carry out ablation study to validate the contributions of individual components to the final

Table 1. Ablation study of the basic components in DRGN on LOL1000 dataset. DL, DA, MSR, KL and SSIM stand for the degradation learning, data augmentation, multi-scale representation, KL divergence and SSIM constraint, respectively.

Model	DL	DA	MSR	\mathcal{L}_{KL}	\mathcal{L}_{ssim}	PSNR	SSIM	FSIM
Input	×	×	×	×	×	12.86	0.610	0.787
w/o DL	×	×	✓	×	✓	19.03	0.857	0.906
w/o DA	✓	×	✓	✓	✓	19.26	0.869	0.912
w/o MSR	✓	✓	×	✓	✓	19.32	0.874	0.910
w/o KL	✓	✓	✓	×	✓	19.61	0.881	0.914
w/o SSIM	✓	✓	✓	✓	×	19.56	0.849	0.907
DRGN	✓	✓	✓	✓	✓	19.88	0.889	0.916



Figure 4. Visualization results of ablation study on LOL1000 dataset. Please refer to the region highlighted in the red box.

enhancement performance. We design three models by removing these three components in turn while keeping the similar computational complexity, termed *w/o DL*, *w/o DA*, and *w/o MSR*. Quantitative results on LOL1000 dataset are tabulated in Table 1, showing that the three modules are complementary. DRGN containing all the modules significantly outperforms its incomplete versions. For example, with both the degradation learning and data augmentation, DRGN gains about 0.85dB and 0.62dB PSNR performance improvements over *w/o DL* and *w/o DA*, respectively. We consider that applying a parametric generator to characterize the implicit distribution of degradation is more reasonable and practical, which avoids the dependence on hand-crafted priors. Furthermore, the training dataset can be automatically augmented and enriched with the newly generated synthetic paired samples, which promote the diversity and abundance of training dataset. On the other hand, using the multi-scale representation strategy is able to cope with the learning tasks in multiple subspaces, thus effectively alleviating the learning difficulty with the joint representation among multi-scale features. The results in Figure 4 also demonstrate that the proposed modules can together produce realistic results with more credible contents and faithful image contrast.

Loss Function. We also evaluate the influence of the KL divergence and SSIM loss on the enhancement performance by training another two models, *w/o KL* (optimized without KL divergence in DeG) and *w/o SSIM* (optimized without SSIM loss in ReG), for comparison. Comparison results on LOL1000 dataset are shown in Table 1 and Figure 4. KL divergence is used to constrain the degradation generator to keep the distribution consistency between the predicted degradation priors $[I_D, I_{D,resf}]$ and accelerate the training.

Table 2. Quantitative performance comparison of the compared methods on Test148 [16]/LOL1000 [37]/VOC144 [8] datasets. LW-DRGN denotes our light-weight model. We also show the number of model parameters (Million), average inference time (Second) and GFlops used for 384×384 images, except for the traditional prior-based algorithm LIME. * denotes that results are obtained with the released test codes directly. The **red**, **blue**, and **green** values respectively indicate the best, second, and third performances.

Methods	LIME [13]	RetinexNet [37]	DeepUPE* [33]	Zero-DCE [12]	KinD [47]	MIRNet [41]	SSIEN [45]	EnlightenGAN [16]	DRGN (Ours)	LW-DRGN (Ours)
PSNR \uparrow	18.35/18.32/19.38	15.45/18.23/18.08	18.41/16.64/19.43	14.42/15.53/15.42	17.27/18.93/22.19	20.34/17.20/19.13	16.23/17.35/18.18	16.34/17.64/19.49	20.41/19.88/22.86	18.85/18.89/20.43
SSIM \uparrow	0.771/0.829/0.757	0.758/0.792/0.749	0.766/0.773/0.781	0.392/0.420/0.348	0.832/0.851/0.834	0.871/0.813/0.781	0.780/0.779/0.727	0.796/0.835/0.790	0.880/0.889/0.858	0.851/0.856/0.839
FSIM \uparrow	0.896/0.871/0.827	0.868/0.860/0.837	0.910/0.865/0.873	0.738/0.741/0.635	0.900/0.908/0.881	0.928/0.872/0.850	0.870/0.830/0.792	0.907/0.884/0.853	0.940/0.916/0.894	0.920/0.886/0.882
Par.(M) \downarrow	—	0.445	0.999	0.079	8.016	31.78	0.486	8.64	4.773	0.660
Time (S) \downarrow	—	0.414	0.016	0.010	0.059	0.630	0.028	0.057	0.152	0.041
GFlops (G) \downarrow	—	83.57	0.214	11.74	78.40	554.32	77.86	37.02	110.59	18.15



Figure 5. Restoration results on LOL1000 [37] (1st and 2nd rows), Test148 [16] (3rd and 4th rows), VOC144 [8] (5th and 6th rows), and real-world scenarios (7th and 8th rows). Our proposed DRGN produces results with better fidelity and naturalness, more faithful to the ground truth. We show more examples of these datasets in the *Supplementary Material*.

SSIM loss can guide the model to produce results with better texture fidelity by enforcing structural similarity. Therefore, compared with *w/o* KL or *w/o* SSIM models, DRGN gains notable improvements in terms of all quality metrics and visual effects.

3.3. Comparison with State-of-the-Arts

Synthetic Data. Eight representative low-light image enhancement methods are employed for comparison. Quantitative results on LOL1000 [37], Test148 [16] and VOC144 [8] datasets are presented in Table 2. Our DRGN significantly outperforms the competing methods among all

quality metrics. In particular, on LOL1000, DRGN outperforms the current SOTA approaches – KinD [47] and EnlightenGAN [16] – in PSNR (SSIM) by 0.95dB (0.038) and 2.24dB (0.054) while enjoying 44.7% more efficiency on parameters. These substantial improvements validate the efficacy of the proposed modules (degradation learning, data augmentation, and multi-scale fusion representation) for the accurate recovery of image content and contrast.

Efficiency also plays an important role in evaluating the model performance for the real-time applications in particular. To this end, we construct a light-weight model, namely LW-DRGN. Specifically, we simplify the multi-resolution

fusion network with the single-branch residual network to reduce the parameter size and the memory footprint. Meanwhile, an attention-guided dense fusion strategy is also used to replace the original skip connection between modules to promote the discriminative representation of multi-stage features. Quantitative results in Table 2 show that LW-DRGN yields an acceptable performance drop while enjoying significantly better efficiency than DRGN by 82.7% and 65.1% in parameter size and inference time, respectively. The high efficiency of LW-DRGN makes it practical for mobile devices and applications requiring real-time throughput. It is worth noting that our proposed LW-DRGN still achieves competitive performance against other low-light enhanced models in both effectiveness and efficiency.

Qualitative comparisons under different low-light conditions (diverse exposures and degradation) on three synthetic low-light datasets are depicted in Figure 5. The results show that DRGN can cope with all low-light cases, generating results with clear and credible details, as well as better fidelity and naturalness. Although the other competitors can light-up contents in the dark regions or produce vivid visual effects (LIME and EnlightenGAN), the predicted results are still corrupted by halo artifacts and noises, and suffer from color distortion as well. For example, as observed from the “Cat” and “House” images in Figure 5, only DRGN restores credible image details and approximates the contrast more similar to the ground-truth, while the competitors fail to solve the degradation and their results exhibit obvious color deviation. Moreover, we observe an interesting phenomenon from these results. The competitors tend to produce brighter outputs no matter what level of degradation (slight or severe degradation conditions), which is just to complete the relighting task using an unified enhanced module (see the first (slight degradation) and third (severe degradation) scenarios in Figure 5). However, DRGN is able to cope with different degradation conditions and produces results with better naturalness and texture fidelity. This is because DRGN takes advantage of the intrinsic degradation priors of the input and employs the data augmentation to improve the training.

Real-world Data. Although recent years have witnessed great progress on the low-light image enhancement task, recovering credible contents and visually pleasing contrast from real-world low-light scenarios is still challenging. Inspired by [22, 27], we conduct experiments on Real63 dataset to further verify the effectiveness of DRGN. Besides two reference-free metrics (NIQE and SSEQ), we also perform a user study to evaluate the performance quantitatively. Specifically, a total of 30 volunteers independently score the visual quality of the enhanced images in the range of 1 to 5 (worst to best quality) in terms of the content naturalness (CN) and color deviation (CD). The quantitative results are included in Table 3. Again, our proposed DRGN

achieves the best and second-best average scores of NIQE and SSEQ. Moreover, DRGN yields the highest average user study scores, including CN and CD for a total of 63 scenarios, surpassing the comparison methods by a large margin. Figure 5 shows the visual comparison results. It is evident that DRGN can infer more realistic and credible image details in the dark regions and well adjust the image contrast, whereas the other methods tend to produce under- or over-exposure results with obvious color distortion (please refer to the “sky” and “plant” in the 7th scenario). These results further confirm that applying the degradation learning and data augmentation can promote robustness and generality on real-world scenarios.

Table 3. Comparison results of perceptual quality on the Real63 dataset. CN and CD are the user study scores. The red and blue values present the best and second performances, respectively.

Methods	RetinexNet	Zero-DCE	KinD	MIRNet	SSIEN	EnlightenGAN	DRGN (Ours)
NIQE ↓	5.192	3.257	3.551	3.287	4.153	4.408	3.051
SSEQ ↓	36.88	23.61	29.48	26.69	32.20	20.08	23.53
CN ↑	2.245	3.147	3.458	3.569	3.026	3.852	4.012
CD ↑	2.263	3.259	3.762	3.625	3.148	3.471	3.984

3.4. Evaluation via Downstream Vision Tasks

Lighting up the image under low-light conditions while recovering credible textural details is meaningful for many high-level vision applications such as object and pedestrian detection. This motivates us to investigate the impact of image enhancement performance on the accuracy of object and pedestrian detection. Therefore, we conduct experiments for the joint image enhancement and object detection tasks. We adopt the real-world low-light dataset (ExDark [25]) as well as synthetic low-light dataset (COCO1000) for evaluation, where the samples are of diverse exposures and degradation and most of them are from night scenes. Our proposed DRGN, KinD [47], Zero-DCE [12], DeepUPE [33], and RetinexNet [37] are directly applied to the low-light samples to generate the predicted normal-light ones. We then use the pre-trained YOLOv4 [1] detector for object detection. Qualitative results, including the image enhancement performance and the precision of object detection, are tabulated in Table 4 (a) and (b). Both the enhancement performance and the detection precision on the predicted normal-light images by DRGN show a significant improvement over the competing low-light enhancement methods, surpassing the top-performing method KinD by 1.91dB and 2.42% in terms of PSNR and mAP on COCO1000 dataset. DRGN also achieves the best results of 63.83% IoU and 67.72% precision on ExDark dataset. Visual comparisons in Figure 6 clearly demonstrate that low-light degradation can greatly affect the readability and recognition, which hinders the object detection accuracy. The enhanced images by our proposed DRGN method ob-

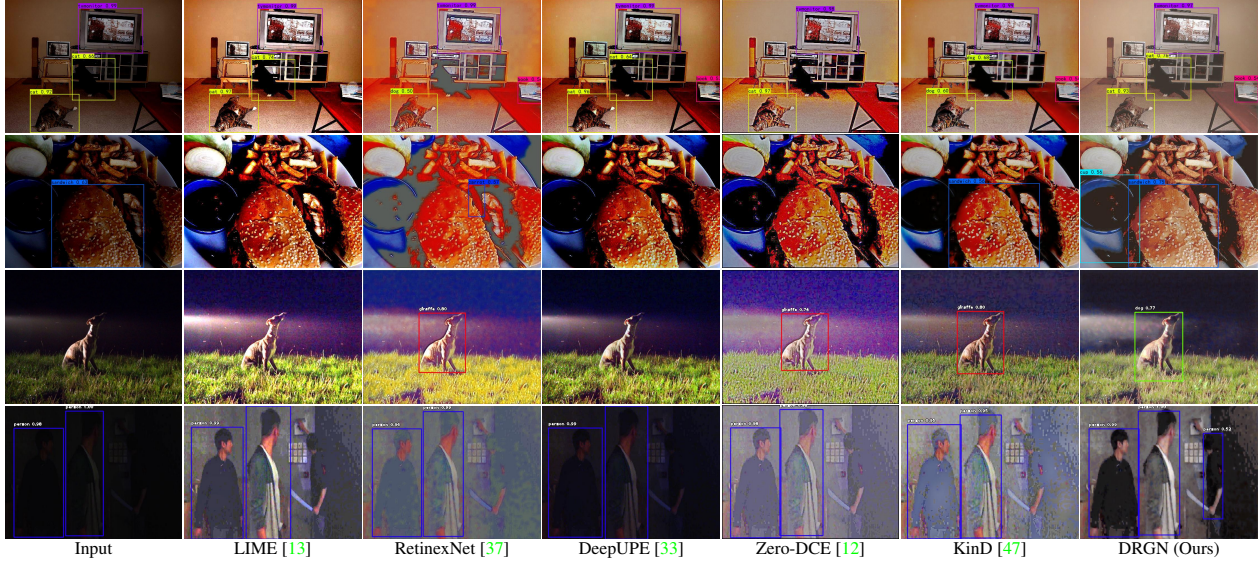


Figure 6. Examples of joint low-light image enhancement and object detection on COCO1000 and ExDark [25] datasets using YOLOv4 [1]. The first two rows show the results of the COCO1000 dataset. Besides relighting up the dark regions to produce visually more authentic results, DRGN detects more objects correctly with high confidence. The last two rows show the results of the ExDark dataset. DRGN is the only algorithm that detects “dog” correctly.

viously promote the detection precision.

We also carry out experiments on a video surveillance dataset collected at night (NightSurveillance [34]) to investigate the effect of low-light enhancement performance on the accuracy of pedestrian detection by using a few popular pedestrian detection algorithms, including ACF [7], RPN+BF [42], Faster R-CNN [44], SDS R-CNN [2] and S3D [35]. In Table 4(c), the enhanced images by DRGN offer a considerable reduction in miss rate (nearly 4%) for these mainstream pedestrian detection approaches. Visual examples of the joint low-light enhancement and pedestrian detection are shown in the *Supplementary Material*.

4. Conclusion

We proposed a novel Degradation-to-Refinement Generation Network (DRGN) for low-light image enhancement. To achieve high-naturalness recovery, we decompose the enhancement task into two stages: degradation learning and content enhancement. By simulating the degradation factors, a number of low/normal-light image pairs can be generated to augment the sample space to promote the training. Moreover, the multi-resolution fusion strategy further improves the feature representation. Consequently, the recovered normal-light images are more realistic with high naturalness due to the degradation learning, data augmentation and multi-scale feature fusion. In particular, we create two low/normal-light datasets (COCO24700 for training and COCO1000 for evaluation) for the joint low-light image enhancement and objective detection tasks. Extensive experimental results on synthetic and real-world low-

Table 4. Comparison results of joint low-light image enhancement, object and pedestrian detection. (a) and (b) are the results on COCO1000 and ExDark [25], respectively. Image Size: 640×480 ; Algorithm: YOLOv4. (c) Miss rate (%) of pedestrian detection on NightSurveillance [34]. We report the results on the original images and enhanced images with our DRGN.

	Methods	RetinexNet	Zero-DCE	KinD	DRGN
Enhancement	PSNR \uparrow	18.32	15.07	18.56	20.47
	SSIM \uparrow	0.723	0.368	0.748	0.790
Detection	Pre. (%)	25.18	25.72	26.54	26.81
	IoU (%)	76.54	76.19	77.01	77.35
	mAP (%)	37.58	41.85	43.49	45.91

(a) COCO1000

	Methods	RetinexNet	Zero-DCE	KinD	DRGN
Enhancement	NIQE \downarrow	5.225	3.825	3.770	3.712
	SSEQ \downarrow	36.98	34.27	36.04	30.65
Detection	Pre. (%)	62.84	63.91	64.86	67.72
	IoU (%)	56.17	58.48	59.29	63.83
	mAP (%)	67.72	68.21	71.45	74.63

(b) ExDark [25]

	ACF	RPN+BF	Faster R-CNN	SDS R-CNN	S3D
w/o DRGN	84.84	82.95	34.56	29.80	26.45
w DRGN	80.82	76.95	30.93	26.86	24.84

(c) NightSurveillance [34]

light samples and downstream vision tasks (e.g., object and pedestrian detection) demonstrate the superiority of DRGN over the competing methods.

References

- [1] Alexey Bochkovskiy, Chien-Yao Wang, and Hong-Yuan Mark Liao. Yolov4: Optimal speed and accuracy of object detection. *CoRR*, abs/2004.10934, 2020. 7, 8, 11
- [2] Garrick Brazil, Xi Yin, and Xiaoming Liu. Illuminating pedestrians via simultaneous detection and segmentation. In *ICCV*, pages 4960–4969, 2017. 8, 11, 17
- [3] Adrian Bulat, Jing Yang, and Georgios Tzimiropoulos. To learn image super-resolution, use a gan to learn how to do image degradation first. In *ECCV*, pages 187–202, 2018. 2
- [4] Holger Caesar, Jasper Uijlings, and Vittorio Ferrari. Coco-stuff: Thing and stuff classes in context. In *CVPR*, pages 1209–1218, 2018. 2, 11
- [5] Jianrui Cai, Shuhang Gu, and Lei Zhang. Learning a deep single image contrast enhancer from multi-exposure images. *IEEE Trans. Image Process.*, 27(4):2049–2062, 2018. 1
- [6] Chen Chen, Qifeng Chen, Jia Xu, and Vladlen Koltun. Learning to see in the dark. In *CVPR*, pages 3291–3300, 2018. 1
- [7] Piotr Dollár, Ron Appel, Serge Belongie, and Pietro Perona. Fast feature pyramids for object detection. *IEEE Trans. Patt. Anal. Mach. Intell.*, 36(8):1532–1545, 2014. 8, 17
- [8] Jianhua Wu Feifan Lv, Feng Lu and Chongsoon Lim. Mblen: Low-light image/video enhancement using cnns. In *BMVC*, 2018. 1, 5, 6, 11, 15
- [9] X. Fu, B. Liang, Y. Huang, X. Ding, and J. Paisley. Lightweight pyramid networks for image deraining. *IEEE Transactions on Neural Networks and Learning Systems*, 31(6):1794–1807, 2020. 4
- [10] Leon A. Gatys, Alexander S. Ecker, and Matthias Bethge. Texture synthesis and the controlled generation of natural stimuli using convolutional neural networks. In *NeurIPS*, 2015. 2
- [11] Michaël Gharbi, Jiawen Chen, Jonathan T Barron, Samuel W Hasinoff, and Frédo Durand. Deep bilateral learning for real-time image enhancement. *ACM Transactions on Graphics (TOG)*, 36(4):1–12, 2017. 1
- [12] C. Guo, C. Li, J. Guo, C. C. Loy, J. Hou, S. Kwong, and R. Cong. Zero-reference deep curve estimation for low-light image enhancement. In *CVPR*, pages 1777–1786, 2020. 1, 4, 5, 6, 7
- [13] X. Guo, Y. Li, and H. Ling. Lime: Low-light image enhancement via illumination map estimation. *IEEE Trans. Image Process.*, 26(2):982–993, 2017. 1, 5, 6
- [14] Wang Hong, Yue Zongsheng, Xie Qi, Zhao Qian, and Meng Deyu. From rain removal to rain generation. In *ECCV*, 2020. 2
- [15] Haidi Ibrahim and Nicholas Sia Pik Kong. Brightness preserving dynamic histogram equalization for image contrast enhancement. *IEEE Trans. Consum. Electron.*, 53(4):1752–1758, 2007. 1
- [16] Yifan Jiang, Xinyu Gong, Ding Liu, Yu Cheng, Chen Fang, Xiaohui Shen, Jianchao Yang, Pan Zhou, and Zhangyang Wang. Enlightengan: Deep light enhancement without paired supervision. *IEEE Trans. Image Process.*, 30:2340–2349, 2021. 1, 2, 4, 5, 6, 11, 14
- [17] Daniel J Jobson, Zia-ur Rahman, and Glenn A Woodell. A multiscale retinex for bridging the gap between color images and the human observation of scenes. *IEEE Trans. Image Process.*, 6(7):965–976, 1997. 1
- [18] Manpreet Kaur, Jasdeep Kaur, and Jappreet Kaur. Survey of contrast enhancement techniques based on histogram equalization. *International Journal of Advanced Computer Science and Applications*, 2(7), 2011. 1
- [19] Wei-Sheng Lai, Jia-Bin Huang, Narendra Ahuja, and Ming-Hsuan Yang. Deep laplacian pyramid networks for fast and accurate super-resolution. In *CVPR*, pages 624–632, 2017. 3
- [20] Edwin H Land. The retinex theory of color vision. *Scientific american*, 237(6):108–129, 1977. 1, 2
- [21] C. Ledig, L. Theis, F. Huszár, J. Caballero, A. Cunningham, A. Acosta, A. Aitken, A. Tejani, J. Totz, Z. Wang, and W. Shi. Photo-realistic single image super-resolution using a generative adversarial network. In *CVPR*, pages 105–114, 2017. 3
- [22] Chulwoo Lee, Chul Lee, and Chang-Su Kim. Contrast enhancement based on layered difference representation. In *ICIP*, pages 965–968, 2012. 5, 7, 11, 15
- [23] Chongyi Li, Jichang Guo, Fatih Porikli, and Yanwei Pang. Lightennet: a convolutional neural network for weakly illuminated image enhancement. *Pattern Recognition Letters*, 104:15–22, 2018. 2
- [24] Lixiong Liu, Bao Liu, Hua Huang, and Alan Conrad Bovik. No-reference image quality assessment based on spatial and spectral entropies. *SPIC*, 29(8):856–863, 2014. 5
- [25] Yuen Peng Loh and Chee Seng Chan. Getting to know low-light images with the exclusively dark dataset. *Comput. Vis. Image Underst.*, 178:30–42, 2019. 2, 5, 7, 8, 11, 12, 13, 16
- [26] Kin Gwn Lore, Adedotun Akintayo, and Soumik Sarkar. Ll-net: A deep autoencoder approach to natural low-light image enhancement. *Pattern Recognition*, 61:650–662, 2017. 1
- [27] Kede Ma, Kai Zeng, and Zhou Wang. Perceptual quality assessment for multi-exposure image fusion. *IEEE Trans. Image Process.*, 24(11):3345–3356, 2015. 5, 7, 11, 15
- [28] Anish Mittal, Rajiv Soundararajan, and Alan C Bovik. Making a “completely blind” image quality analyzer. *IEEE Signal Process. Lett.*, 20(3):209–212, 2012. 5
- [29] V. Pappayan and M. Elad. Multi-scale patch-based image restoration. *IEEE Trans. Image Process.*, 25(1):249–261, 2016. 4
- [30] Wenqi Ren, Sifei Liu, Lin Ma, Qianqian Xu, Xiangyu Xu, Xiaochun Cao, Junping Du, and Ming-Hsuan Yang. Low-light image enhancement via a deep hybrid network. *IEEE Trans. Image Process.*, 28(9):4364–4375, 2019. 1
- [31] Liang Shen, Zihan Yue, Fan Feng, Quan Chen, Shihao Liu, and Jie Ma. Msr-net: Low-light image enhancement using deep convolutional network. *arXiv preprint arXiv:1711.02488*, 2017. 2
- [32] Yunhang Shen, Rongrong Ji, Zhiwei Chen, Xiaopeng Hong, Feng Zheng, Jianzhuang Liu, Mingliang Xu, and Qi Tian. Noise-aware fully webly supervised object detection. In *CVPR*, pages 11323–11332, 2020. 1
- [33] Ruixing Wang, Qing Zhang, Chi-Wing Fu, Xiaoyong Shen, Wei-Shi Zheng, and Jiaya Jia. Underexposed photo enhance-

- ment using deep illumination estimation. In *CVPR*, pages 6849–6857, 2019. 1, 2, 5, 6, 7
- [34] Xiao Wang, Jun Chen, Zheng Wang, Wu Liu, Shin’ichi Satoh, Chao Liang, and Chia-Wen Lin. When pedestrian detection meets nighttime surveillance: A new benchmark. In *IJCAI*, pages 509–515, 2020. 2, 5, 8, 12, 17
- [35] Xiao Wang, Chao Liang, Chen Chen, Jun Chen, Zheng Wang, Zhen Han, and Chunxia Xiao. S3d: Scalable pedestrian detection via score scale surface discrimination. *IEEE Trans. Circuits Syst. Video Technol.*, 30(10):3332–3344, 2020. 8, 11, 17
- [36] Zhou Wang, Alan C Bovik, Hamid R Sheikh, and Eero P Simoncelli. Image quality assessment: from error visibility to structural similarity. *IEEE Trans. Image Process.*, 13(4):600–612, 2004. 3
- [37] Chen Wei, Wenjing Wang, Wenhan Yang, and Jiaying Liu. Deep retinex decomposition for low-light enhancement. In *BMVC*, page 155, 2018. 1, 2, 5, 6, 7, 11, 14
- [38] Jung-Hsuan Wu and Suguru Saito. Interactive relighting in single low-dynamic range images. *ACM TOG*, 36(2):1–18, 2017. 2
- [39] Wenhan Yang, Shiqi Wang, Yuming Fang, Yue Wang, and Jiaying Liu. From fidelity to perceptual quality: A semi-supervised approach for low-light image enhancement. In *CVPR*, pages 3063–3072, 2020. 4
- [40] Huanjing Yue, Jingyu Yang, Xiaoyan Sun, Feng Wu, and Chunping Hou. Contrast enhancement based on intrinsic image decomposition. *IEEE Trans. Image Process.*, 26(8):3981–3994, 2017. 2
- [41] Syed Waqas Zamir, Aditya Arora, Salman Khan, Munawar Hayat, Fahad Shahbaz Khan, Ming Hsuan Yang, and Ling Shao. Learning enriched features for real image restoration and enhancement. In *ECCV*, pages 492–511, 2020. 1, 2, 5, 6
- [42] Liliang Zhang, Liang Lin, Xiaodan Liang, and Kaiming He. Is faster R-CNN doing well for pedestrian detection? In *ECCV*, pages 443–457, 2016. 8, 11, 17
- [43] Lin Zhang, Lei Zhang, Xuanqin Mou, and David Zhang. Fsim: A feature similarity index for image quality assessment. *IEEE Trans. Image Process.*, 20(8):2378–2386, 2011. 5
- [44] Shanshan Zhang, Rodrigo Benenson, and Bernt Schiele. Citypersons: A diverse dataset for pedestrian detection. In *CVPR*, pages 4457–4465, 2017. 8, 11, 17
- [45] Yu Zhang, Xiaoguang Di, Bin Zhang, and Chunhui Wang. Self-supervised image enhancement network: Training with low light images only. *arXiv e-prints*, pages arXiv–2002, 2020. 1, 5, 6
- [46] Yulun Zhang, Kunpeng Li, Kai Li, Lichen Wang, Bineng Zhong, and Yun Fu. Image super-resolution using very deep residual channel attention networks. In *ECCV*, pages 286–301, 2018. 4
- [47] Yonghua Zhang, Jiawan Zhang, and Xiaojie Guo. Kindling the darkness: A practical low-light image enhancer. In *ACM MM*, pages 1632–1640, 2019. 1, 2, 5, 6, 7
- [48] Zhedong Zheng, Xiaodong Yang, Zhiding Yu, Liang Zheng, Yi Yang, and Jan Kautz. Joint discriminative and generative learning for person re-identification. In *CVPR*, pages 2138–2147, 2019. 1
- [49] Minfeng Zhu, Pingbo Pan, Wei Chen, and Yi Yang. Eemefn: Low-light image enhancement via edge-enhanced multi-exposure fusion network. In *AAAI*, pages 13106–13113, 2020. 1

Supplementary Material

The following items are included in this supplementary material.

- The details of the discriminator in DRGN.
- Analysis and visualization on the degradation model.
- Examples of the synthetic low-light samples.
- More visual results of low-light image enhancement.
- More visual results of detection.

A. Details of the Discriminator

Figure 7 shows the detailed architectures of the discriminators \mathcal{D}_{low} and \mathcal{D}_{de} in our method. These two discriminators employ the same architecture for convenience. More specifically, each of them contains an initial convolution layer, four sampling units to extract the deep features (a strided convolution to enlarge the receptive field and a 1×1 convolution to fuse the channel features), a global average pooling and a fully connected layer to produce the logical prediction.

B. Analysis and Visualization on the Degradation Model

To better understand the degradation learning in the first stage, we show the examples of the predicted degradation in Figure 8. In particular, the degradation simulated by the generator is from the low-light dataset (Test148 [16]), where the samples are of diverse exposures and degradation under different scenarios. We can see that our proposed DRGN can adaptively characterize the degradation itself from the low-light inputs rather than learning a unified degradation pattern (please refer to the third column). To maintain the diversity and reality of the degradation, we introduce GAN loss and consistency loss (the KL Divergence) to regularize both predicted degradation $[I_D, I_{D,ref}]$ and low-light image pair $[I_L, I_{L,ref}]$ to be with similar distributions. In addition, we also show the visualization of the degradation learning and content refinement in Figure 9, including the results of predicted degradation ($I_D, I_{D,ref}$), synthetic low-light images ($I_{L,ref}$), intermediate results ($I_B, I_{B,ref}$) as well as final predicted normal-light images (I^*, I_{ref}^*).

C. Examples of the Synthetic Low-light Samples

In our main paper, we employ a parametric generator to extract the degradation from the low-light input. By this way, we can create any number of paired low-light samples by performing the degradation on the additional reference samples via $I_{L,ref} = I_{L,ref} = I_D + \psi(I_{ref}^*, I_D)$, where I_{ref}^* denotes the **strictly high-quality** version of I_{ref} , and $\psi(I_{ref}^*)$ is equal to I_{ref} , generated via $\psi(\cdot)$ and I_D . To this

end, we also introduce two novel low/normal-light datasets (COCO24700 for training and COCO1000 for evaluation) based on COCO [4] dataset, which can be used for the joint low-light image enhancement and detection tasks under extreme degradation scenarios. The degradation factors are extracted from the real-world low-light samples (Ex-Dark [25]), which cover 7363 scenarios with diverse real degradation factors, and at the same time have complex image contents and imaging conditions such as night scenes. More specifically, by applying the predicted degradation factors to the referenced high-quality images, we create the synthetic low-light samples. Under the supervision of the GAN loss and consistency loss (the KL Divergence), consequently, our synthetic low-light images are more realistic with better naturalness, more faithful to the real distribution of low-light images than the images generated via hand-crafted rendering techniques. The synthetic examples of the low-light image dataset are shown in Figure 10. In particular, we can control the strength of the degradation performed on the target referenced image to generate a set of paired samples with different degradation densities. As shown in Figure 10, the image gets heavier and severer degradation effects from the top to bottom. Therefore, we can create any required number of low-/normal-light paired samples with diverse degradation strengths based on the existing detection or segmentation datasets.

D. More Visual Results of Low-light Image Enhancement

We provide more visual comparison results to show the performance of our proposed Degradation-to-Refinement Generation Network (DRGN) and other five state-of-the-art methods. The comparisons are conducted on several benchmark datasets, including the synthetic low-light image datasets, LOL1000 [37], Test148 [16], and VOC144 [8]), as well as the real-world low-light dataset, Real63 [22, 27]. More visual results are given in Figures 11, 12, 13 and 14. We can see that the competing methods tend to produce under- or over-exposure results with obvious color distortions. In contrast, our proposed DRGN method is able to cope with different levels of degradation, and produces results with better fidelity and naturalness. In particular, DRGN can recover more realistic and credible image details under the dark regions with more plausible image contrast.

E. More Visual Results of Detection

To investigate the effect of low-light image enhancement performance on the accuracy of high-level vision tasks such as object and pedestrian detection, we introduce the popular benchmark algorithms (YOLOv4 [1] for object detection, RPN+BF [42], Adapted Faster R-CNN [44], SDS R-CNN [2] and S3D [35] for pedestrian detection) and low-

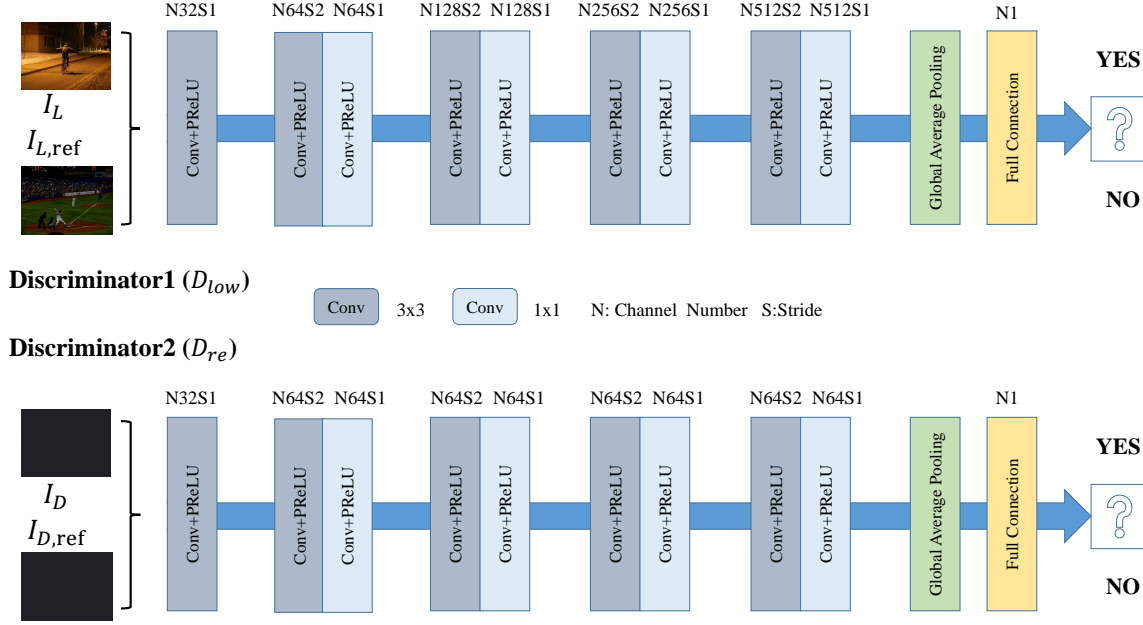


Figure 7. Architecture of the discriminators (\mathcal{D}_{low} and \mathcal{D}_{de}).

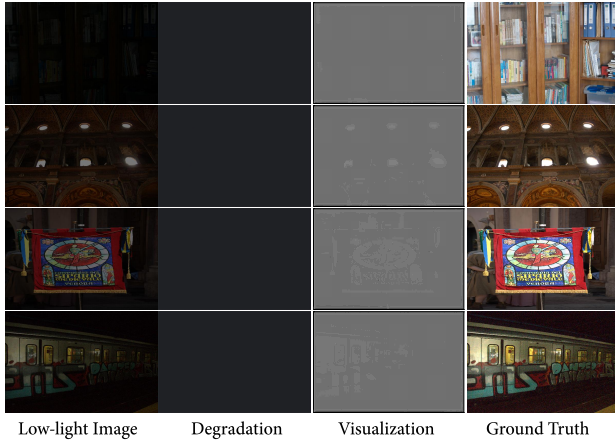


Figure 8. Visualization of the degradation learning. The first and the last columns refer to the low-light input and normal-light images, respectively. The second column denotes the learned degradation factor. For a better visual effect, we rescale the pixel values of degradation images into three values (0, 128, 255), and produce the visual presentation in the third column. It reflects the strength of the degradation at each pixel location. The lower the pixel value is, the more severe the low-light degradation.

light datasets (ExDark [25] for object detection and Night-Surveillance [34] for pedestrian detection) for these tasks. Visual comparison results are presented in Figures 15 and 16.



Figure 9. Visual presentation of DRGN on real-world ExDark [25] dataset. I_L and $I_{L,ref}$ are the predicted degradation from the original and synthetic low-light inputs (I_L , $I_{L,ref}$), respectively. I_B and $I_{B,ref}$ are the corresponding intermediate results. The second stage takes (I_B , $I_{B,ref}$) as inputs to refine the color, contrast, and textural details, and produces the enhanced outputs (I^* , I_{ref}^*). I_D is the predicted degradation.



Figure 10. Visualization of the synthetic low-light images by the degradation generator (DeG). In particular, by applying different degradation strengths to the referenced target image, we can create a set of degradation images corresponding to different and consecutive degradation effects (the image gets severer degradation effects from the top to bottom).

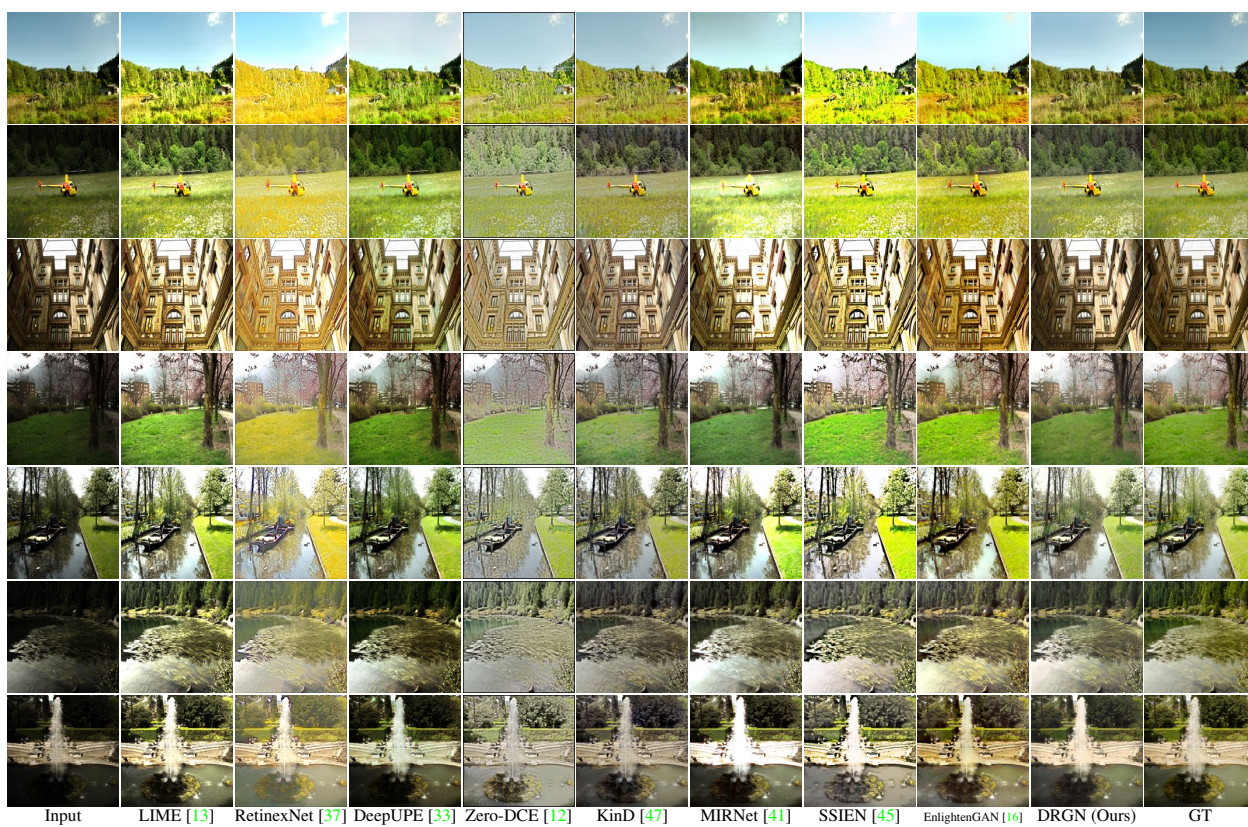


Figure 11. More restoration results on LOL1000 [37] dataset.

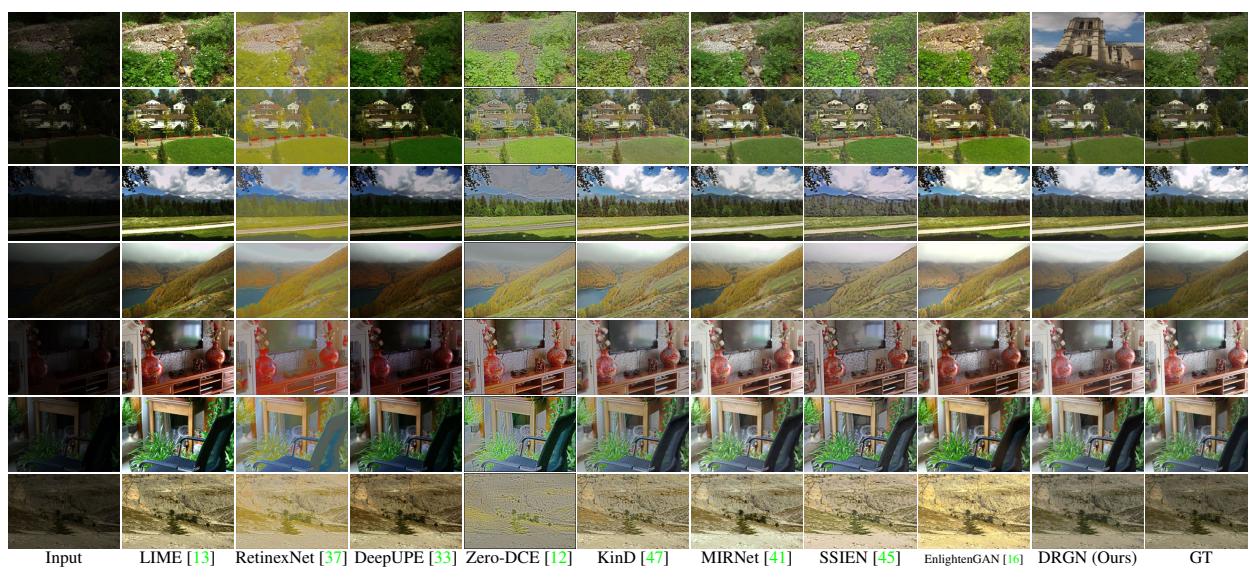


Figure 12. More restoration results on Test148 [16] dataset.

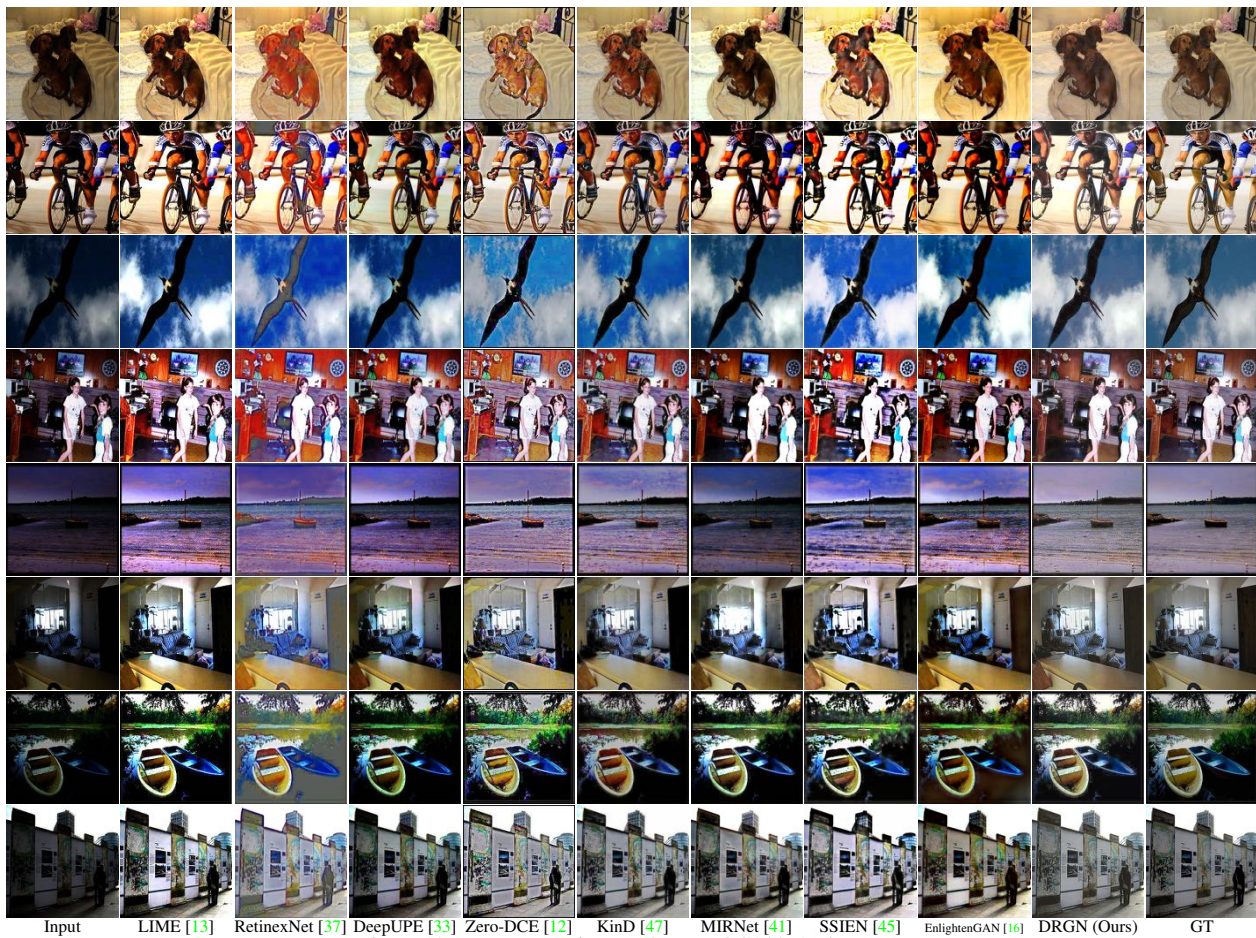


Figure 13. More restoration results on VOC144 [8] dataset.

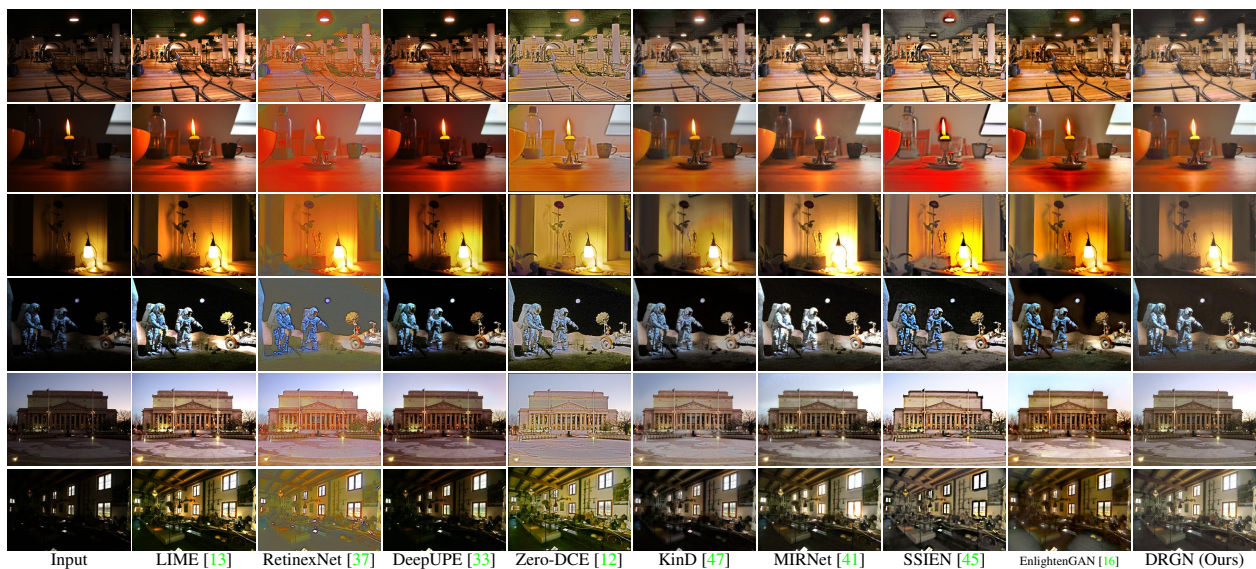


Figure 14. More restoration results on Real63 [22, 27] dataset.



Figure 15. Visualization of the object detection results on ExDark [25] Dataset.

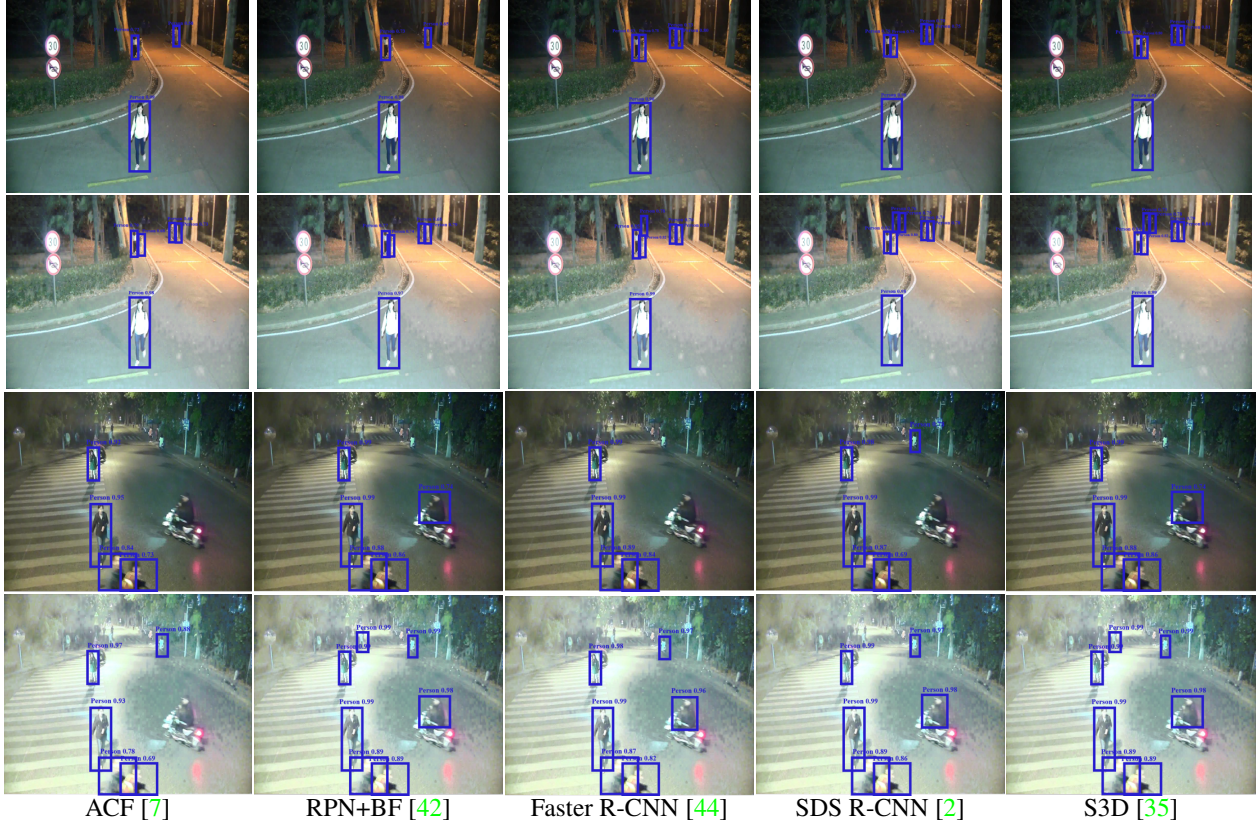


Figure 16. Examples of joint low-light image enhancement and pedestrian detection on NightSurveillance [34] dataset based on some popular algorithms, including ACF [7], RPN+BF [42], Adapted Faster R-CNN [44], SDS R-CNN [2] and S3D [35]. The first and third rows show the detection results of these detectors on the original night images while the second and fourth rows are the results of the enhanced images by our DRGN method, respectively. Our method benefits all detectors by capturing more pedestrians with better detection accuracy.